Environ Monit Assess (2016) 188:119
DOI 10.1007/s10661-015-5045-x

Soil salinity detection from satellite image analysis: an integrated approach of salinity indices and field data

Md. Manjur Morshed · Md. Tazmul Islam · Raihan Jamil

Received: 11 June 2015 / Accepted: 10 December 2015

Abstract This paper attempts to detect soil salinity from satellite image analysis using remote sensing and geographic information system. Salinity intrusion is a common problem for the coastal regions of the world. Traditional salinity detection techniques by field survey and sampling are time-consuming and expensive. Remote sensing and geographic information system offer economic and efficient salinity detection, monitoring, and mapping. To predict soil salinity, an integrated approach of salinity indices and field data was used to develop a multiple regression equation. The correlations between different indices and field data of soil salinity were calculated to find out the highly correlated indices. The best regression model was selected considering the high R^2 value, low P value, and low Akaike's Information Criterion. About 20 % variation was observed between the field data and predicted EC from the satellite image analysis. The precision of this salinity detection technique depends on the accuracy and uniform distribution of field data.

Keywords Salinity indices · Regression · Landsat image · Remote sensing · Bangladesh

M. M. Morshed (✉) · M. T. Islam · R. Jamil
Department of Urban and Regional Planning, Khulna University of Engineering & Technology, LE-303, Khulna 9203, Bangladesh
e-mail: manjurmorshedkhan@gmail.com

M. T. Islam
e-mail: tazmulislambabu@yahoo.com

R. Jamil
e-mail: rjamil.kueturp10@gmail.com

Introduction

This paper attempts to measure soil salinity from satellite image analysis. Salinity usually refers to a significant concentration of mineral salts in soil or water because of the hydrological processes (Schofield et al. 2001). There are two main types of salinization: primary and secondary (Mashimbye 2013). Primary salinization occurs through the natural processes, e.g., flood and storm surge. Secondary salinization occurs due to poor management practices, e.g., excessive use of fertilizer (Wu et al. 2008).

Salinization is one of the most common land degradation processes in coastal regions, especially in arid and semi-arid areas. It is one of the oldest environmental problems and one of the main paths to desertification (Kassas 1987). Excessive accumulation of soluble salts in the soil surface influences soil properties, which decreases soil productivity, limits the growth of crops, and constrains agricultural productivity (Table 1). Excessive concentration of salts in soil may lead to the abandonment of agricultural land (Li et al. 2011).

There are extensive salt-affected areas in all the continents, but accurate data concerning salt-affected areas is rather scarce (Gupta and Abrol 1990). Statistics about the

Published online: 27 January 2016

Table 1 General ranges of plant tolerance to soil salinity

Salinity (EC, $dS.m^{-1}$)	Plant response
0 to 2	Mostly negligible
2 to 4	Growth of sensitive plants may be restricted
4 to 8	Growth of many plants is restricted
8 to 16	Only tolerant plants grow satisfactorily
Above 16	Only a few, very tolerant plants grow satisfactorily

(Source: Khaier 2003)

extent of the world's salt-affected areas vary according to the authors. However, a general estimate of salt-affected area is close to one billion hectares, about 7 % of the earth's continental extent (Abdelfattah et al. 2009). About 77 million hectares of land have been salinized because of human activities (secondary salinization), and every year, it continues to spread at a rate of up to two million hectares around the world (Garcia et al. 2005). Globally, the cost of irrigation-induced salinity is equivalent to an estimated US$11 billion per year globally (FAO 2005).

To keep track of the changes in salinity and anticipate further degradation, mapping and monitoring are essential for proper and timely decision making to adjust management practices and undertake proper reclamation and rehabilitation measures (Nwer et al. 2013). Conventional means of salinity detection by surveying requires a great deal of time and expense. Geographic information system (GIS) technique and remote sensing (RS) data has become an economic and efficient tool for detecting, mapping, and monitoring salt-affected areas along with its spatial and temporal variations (Ben-Dor et al. 2002; Aldabaa et al. 2014).

Literature review

Various RS data are being used for identifying and monitoring salt-affected areas such as aerial photographs, video images, infrared thermography, visible and infrared multispectral, and microwave images (Metternicht and Zinck 2003). Landsat imagery is often used because it offers a wide range of bands and allows image enhancement for detecting surface features. Several authors have

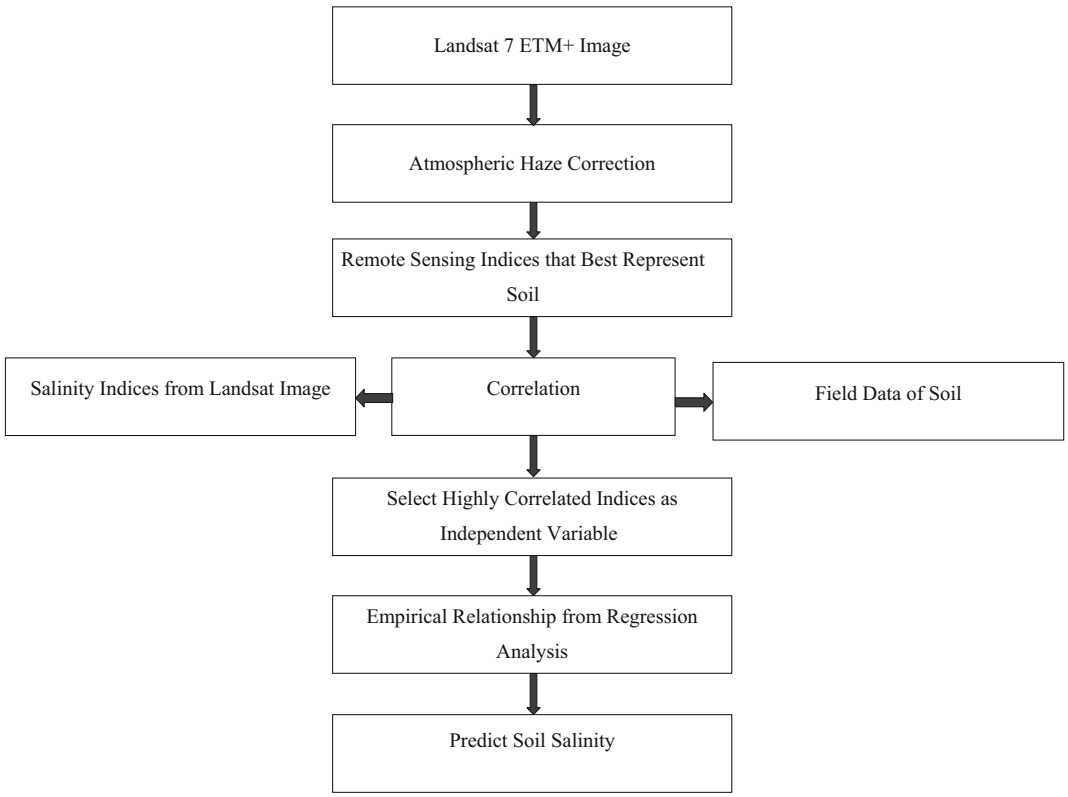

Fig. 1 Proposed integrated approach for soil salinity detection

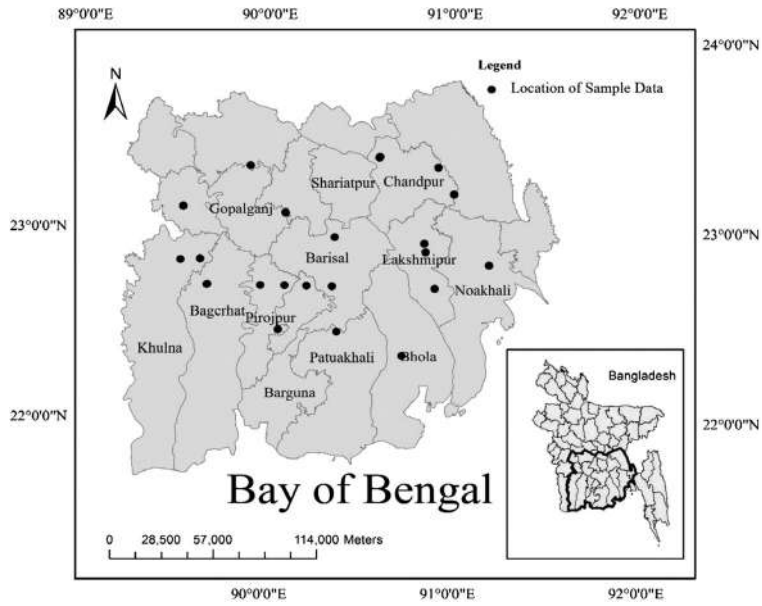

Fig. 2 Location of the study area and sample data

demonstrated the advantage of combining Satellite image analysis with field data to assess the accuracy of salinity detection (Bishop and McBratney 2001; Carre and Girard 2002; Bouaziz et al. 2011).

Bouaziz et al. (2011) used the Pearson correlation between the field data of soil salinity (electrical conductivity (EC) expressed in decisiemens/meter) and 18 salinity indices. They found that salinity index SI_2 and near-infrared (NIR) band are highly correlated with the field EC. They used SI_2 and NIR band indices in a regression equation to predict soil salinity, which proved to be quite accurate for satellite image-based salinity detection technique for spectral, spatial, and temporal variations. Khan et al. (2001) calculated the soil salinity indices and performed principal component analysis (PCA) to predict soil salinity.

Garcia et al. (2005) directly used the blue band, near-infrared (NIR) band, normalized difference vegetation index (NDVI), and near-infrared (NIR)/red (band 4/band 3) ratio in the regression equation to measure soil salinity. They conducted three regression models—namely ordinary least squares (OLS), spatial autoregression (SAR), and spatial lag model (SLAG)—and selected a model for salinity prediction considering low P value, high R^2, and low standard error.

From the above discussion, different bands of satellite image provide varying levels of accuracy (correlation indices) in detecting salinity. This however indicates that working with available multiple indices can be an option to increase the accuracy in calculating soil salinity. Therefore, experimentation with the satellite image analysis and cross-checking with the field data can direct to an alternative and accurate salinity detection technique.

Materials and methods

Proposed integrated approach

This research proposed an integrated approach of salinity indices and field data to develop a multiple regression equation for predicting soil salinity from satellite image analysis. The overall working procedure is in Fig. 1.

Study area and data collection

Southern regions of Bangladesh are especially vulnerable to salinity intrusion. South and south-western districts of

Table 2 Corrected haze value in different bands

Band	DN (haze)
1	35.000
2	11.749
3	7.923
4	4.527
5	14.910
7	3.014

Bangladesh—*Khulna*, *Patuakhali*, *Pirojpur*, *Barisal*, *Bagerhat*, *Noakhali*, *Lakshmipur*, *Chandpur*, *Bhola*, and *Gopalgonj*—have been selected as the study area (Fig. 2). Very high soil salinity was reported from *Khulna*, *Bagerhat*, *Satkhira*, *and Patuakhali* districts (SRDI 2010). In addition, several studies had indicated that the study area was severely affected by a number of natural calamities (e.g., storm surges) that caused salinity intrusion (Ortiz 1994; Khan et al. 2000; WB 2000; Singh et al. 2001).

Field data (EC) of soil salinity (84 samples) of different geographical coordinates of the study area were collected from the Institute of Water Modeling (IWM), Bangladesh (Table 2). These field samples were collected during the dry season (April–May) of 2012 and 2013. A Landsat 7 ETM+ image (path 137, row 44) on November 27, 2012 was collected from the United States Geological Survey (USGS). Field data of soil salinity was not available close to the satellite image acquisition date. Due to the highly uneven distribution and duplicate data within similar geographical coordinates, out of 84 field samples of soil salinity, 40 were used in this analysis. In Fig. 2, 40 sample data were shown in 21 locations.

Salinity calculation from field data

The most common methods used for calculating soil salinity from field data are (i) electrical conductivity (EC); (ii) total soluble salts (TSS) or total dissolved salts (TDS); (iii) sodium adsorption ratio (SAR); and (iv) exchangeable sodium percentage (ESP). The samples collected from the Institute of Water Modeling (IWM), Bangladesh, were in TDS form. IWM measured TDS of soil solution based on the saturated paste of soil and water. The TDS was converted into EC using the following formulas:

i. $\text{If EC} < 5\,\text{dS/m},\ \text{TDS(mg/L)} = 640 * \text{EC(dS/m)};$

ii. $\text{If EC} > 5\ \text{dS/m},\ \text{TDS(mg/L)} = 840 * \text{EC(dS/m)}$ (Hanson et al. 2006).

Image correction

Three satellite image correction processes were followed to gain accurate information about the surface features. Firstly, Landsat 7 ETM+ image gap due to the scan line corrector (SLC) failure from May 31, 2003, was filled. Secondly, accurate information of the earth surface is not recorded in satellite image due to the presence of different kinds of particles in the atmosphere. An improved dark-object subtraction technique for atmospheric scattering correction (haze value correction) of multispectral data by Chavez (1988) was used to gain better information from the satellite images. The corrected haze values in different bands are shown in Table 3.

Thirdly, all the data recorded in digital number (DN) were converted into reflectance. Huang et al. (2002) found that noise from reflectance was 50 % less than noise from DN value. To do so, first, DN values were converted into radiance by considering gain and bias of different bands using the following expression:

$$L = (\text{gain} * \text{DN}) + \text{bias};$$

here, L is radiance.

Thereafter, the radiance was converted to reflectance by considering Earth-Sun distance and Sun elevation using the following expression:

$$R = \frac{\pi \times L \times d^2}{E \times \theta_{se}},$$

where

R reflectance
L radiance
d Earth-Sun distance (depends on the day of image acquisition)
θ_{se} sun elevation in radian

Table 3 Regression models between field EC and selected salinity indices

Variable		OLS	SLAG	SAR
	R2	0.77	0.79	*0.82*
	Residual standard error	1.212	1.12	*1.0226*
Intercept	Coefficient	14.93	14.56	12.53
	P value	0.0136	0.006	0.000
NIR	Coefficient	1500.09	1483.82	1108.95
	P value	0.0005	0.0004	0.000
IR/R	Coefficient	3.93	3.86	2.73
	P value	0.000	0.001	0.001
SI-2	Coefficient	−979.64	−964.97	−717.86
	P value	0.005	0.0017	0.031
SAVI	Coefficien	−395.64	−393.51	−295.7
	P value	0.001	0.001	
Lambda	Coefficient			0.63
	P value			0.00001
AICC		133.948	134.95	*128.363*

P value = 5%

The image acquisition dates and its respective values are available in the table by Chander et al. (2009).

Index selection and correlation

Thirteen salinity indices were selected for this study from a comprehensive literature review (Bouaziz et al. 2011; Garcia et al. 2005; Khan et al. 2001).

$$\text{Salinity index one}: \quad \text{SI\_1} = \sqrt{\text{GREEN} + \text{RED}} \tag{1}$$

$$\text{Salinity index two}: \quad \text{SI\_2} = \sqrt{\text{GREEN}^2 + \text{RED}^2 + \text{NIR}^2} \tag{2}$$

$$\text{Salinity index three}: \quad \text{SI\_3} = \sqrt{\text{GREEN}^2 + \text{RED}^2} \tag{3}$$

$$\text{Salinity index eleven}: \quad \text{SI\_11} = \frac{\text{SWIR1}}{\text{SWIR2}} \tag{4}$$

$$\text{Intensity index one}^2\text{: INT\_1} = \frac{(\text{GREEN} + \text{RED})}{2} \tag{5}$$

$$\text{Intensity index two}^3\text{: INT\_2} = \frac{(\text{GREEN} + \text{RED} + \text{NIR})}{2} \tag{6}$$

$$\text{Brightness index}^4\text{:} \quad \text{BI} = \sqrt{\text{GREEN}^2 + \text{NIR}^2} \tag{7}$$

Soil adjusted vegetation index[5]:

$$\text{SAVI} = \frac{(\text{NIR} - \text{RED}) \times (1 + L)}{(\text{NIR} + \text{RED} + L)} \tag{8}$$

[1] SI_1, SI_2, SI_3, and SI_11 are the calculation of intensity value of the image or soil indices. High index value indicates high reflectance, thus high soil salinity.

[2] INT_1: Intensity within the visible spectral range.

[3] INT_2: Intensity within the VIS-NIR spectral range.

[4] BI: It is designed to detect soil brightness, which is often associated with soil salinity.

[5] SAVI: The soil-adjusted vegetation index was developed as a modification of the Normalized Difference Vegetation Index (NDVI) to correct for the influence of soil brightness when vegetative cover is low. The SAVI is structured similar to the NDVI but with the addition of a soil brightness correction factor.

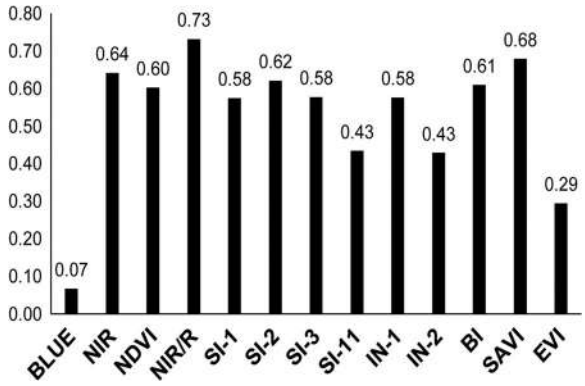

Fig. 3 Correlation between field data and soil salinity indices

Here, constant $L = 0.5$; the value of L varies with location. In high-vegetation regions, $L = 0$; in low vegetation regions, $L = 1$. However, $L = 0.5$ works in most situation and is used as default value (Huete et al. 1985).[6]

Normalized difference vegetation index[7]:

$$\text{NDVI} = \frac{\text{NIR} - \text{RED}}{\text{NIR} + \text{RED}} \tag{9}$$

$$\text{Enhanced vegetation index}: \quad \text{EVI} = 2.5 \times \frac{\text{NIR} - \text{RED}}{\text{NIR} + c1 \times \text{RED} - c2 \times \text{BLUE} + L} \tag{10}$$

where $c1 = 6$, $c2 = 7.5$, and $L = 1$; these are the coefficients to correct atmospheric condition, i.e., aerosol resistance (Vermote et al. 2002).

$$\text{The ratio of two spectral bands(band 3 and band 4)} = \frac{\text{NIR}}{\text{RED}} \tag{11}$$

$$\text{blue band} \tag{12}$$

$$\text{and NIR band} \tag{13}$$

These thirteen indices were calculated from the corrected image in ERDAS model maker. The correla-

[6] NDVI: The normalized difference vegetation index (NDVI) is an index of plant greenness or photo synthetic activity. The high value of NDVI indicates that a high portion of the radiation is absorbed by vegetation. NDVI value ranges from minus one (-1) to plus one (+1).

[7] EVI: The enhanced vegetation index (EVI) corrects some distortions in the reflected light caused by the particles in the air as well as the ground cover below the vegetation.

Table 4 Comparative area in different salinity levels

Salinity class	Range of EC (ds/m)	Total (Sq. km)	Percentage
Non-saline (EC, <1)	Less than 1	390.08	9.13
Very low saline (EC, 1–2)	1 to 2	442.43	10.35
Low saline (EC, 2–4)	2 to 4	1331.92	31.17
Medium (EC, 4–6)	4 to 6	1281.61	29.99
High (EC, 6–8)	6 to 8	649.76	15.21
Very high (EC, >8)	Greater than 8	177.45	4.15
Total (Sq. km)		4273.25	100.00

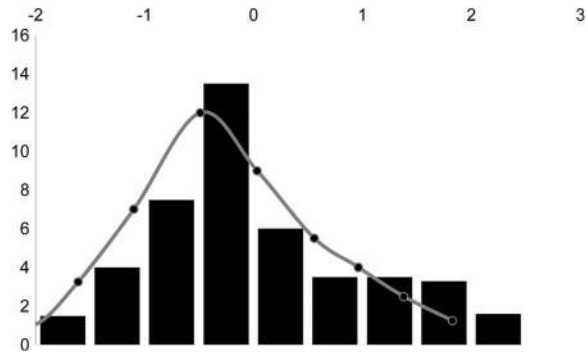

Fig. 5 Histogram of residuals

tions between these indices and field data of soil salinity (EC) were calculated to find out the highly correlated indices (Fig. 3).

Infrared bands of the satellite image as well as SI_2, NIR/R, and SAVI were highly correlated with the field (EC) samples.

Analysis and findings

Regression model

Stepwise regression was done to determine the combination of bands that showed the best correlation with the field EC values. OLS, SAR, and SLAG were used as regression models to develop a multiple regression equation. Highly correlated indices were used as independent variables to predict soil salinity in multiple regression equation. The regression model calculations were done using GeoDa software, and the results are shown in Table 4. SAR and SLAG were performed by creating a spatial weight file. The weight file was created by selecting an appropriate weight function based on model fit (maximum likelihood criterion) and by analyzing how well the model accounted for autocorrelation in the residuals.

The SAR model was selected for regression analysis considering the highest R^2 value, low P and AIC value, and low standard error. The regression equation combining salinity indices is shown in Eq. 14. The regression analysis considered 5 % level of significance. The comparison between field and predicted salinity (EC) is in the appendix table.

$$\text{Salinity} = 12.53 + 1108.95 * \text{NIR} + 2.73 * \text{NIR/R} - 717.86 * \text{SI2} - 295.7 * \text{SAVI} \quad (14)$$

Figure 4 illustrated that most of the predicted EC were close to the field data. The predicted EC values deviated from the normal trend line were not addressed by the linear regression equation.

From Fig. 5, it was observed that the histogram of residuals was very close to a normal distribution; meaning, there was no correlation among the residuals and

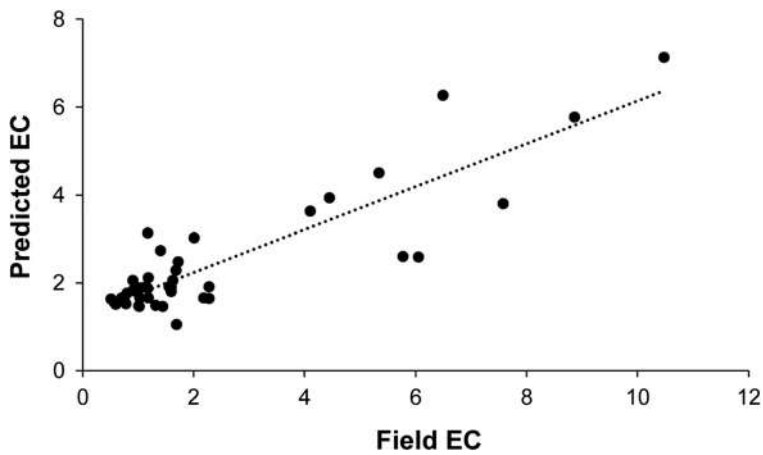

Fig. 4 Relation between field EC and predicted EC from regression equation

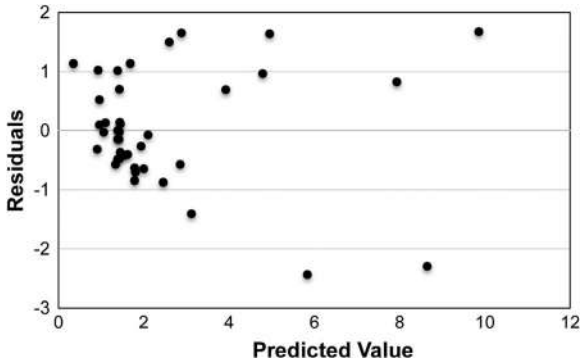

Fig. 6 Predicted value versus residuals

these were spatially independent. Also, Fig. 6 showed that there was no correlation among the residuals when calculating predicted EC and these were also spatially independent.

Soil salinity

The spectral characteristics of different salinity classes are shown in Fig. 7. From the figure, the NIR and SWIR bands were found to be sensitive in different salinity classes. These bands help to differentiate saline and non-saline classes. In addition, a slight variation of reflectance was observed in various levels of soil salinity.

The soil salinity was predicted by applying the above multiple regression Eq. (14) that represented soil salinity quite accurately (Table 5). The salinity map was classified in seven classes, where EC ranged from non-saline to heavy saline soil. Water body was excluded from the salinity classes and is shown in another class by denoting a null value to it.

From Table 4, about 4.15 % of the total land of the study area was severely and about 15 % was highly affected by salinity. Such levels of salinity restrict the growth of crops—only saline tolerable crops can be cultivated here. About 19 % of the total land area was moderately saline affected, which restricts the growth of saline sensitive crops. About 31 % of the total area was found to have low soil salinity (2–4 dS/m). The remaining 50 % of the soil was slightly or not affected by salinity.

Figure 8 showed the spatial distribution of soil salinity in the study area. The figure showed that land areas beside the rivers were highly and moderately saline affected because of the salinity intrusion from the Bay of Bengal through various rivers and their tributaries. Upper parts of the study area were slightly or not affected at all by salinity.

Conclusion

This paper has presented the potential of integrating Landsat image analysis and field survey data to assess and monitor soil salinity over a large area. Although the correlations between the field EC and salinity indices did not have the best results, the comparison of three spatial regression models and selection of the best model provided accuracy in the salinity detection. About 20 % variation was observed between the field data and predicted EC from the image analysis. The precision of this integrated approach mostly depends on the accuracy of the field data. The data used in this research were not uniformly distributed across the study area, and the

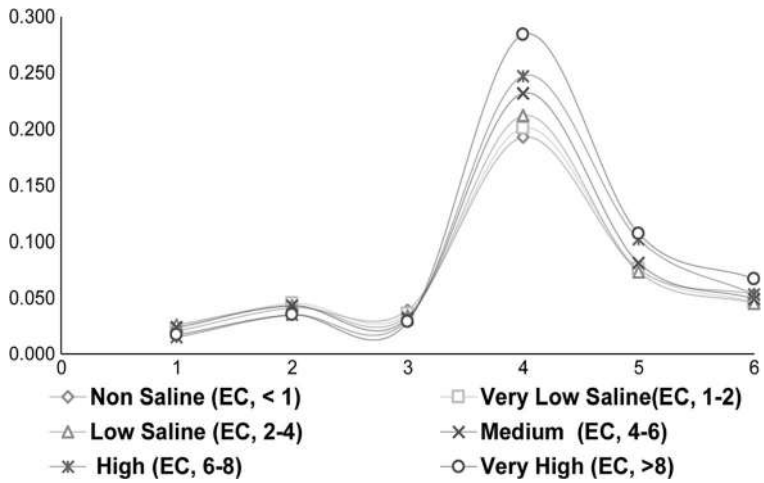

Fig. 7 Reflectance characteristics in different salinity levels

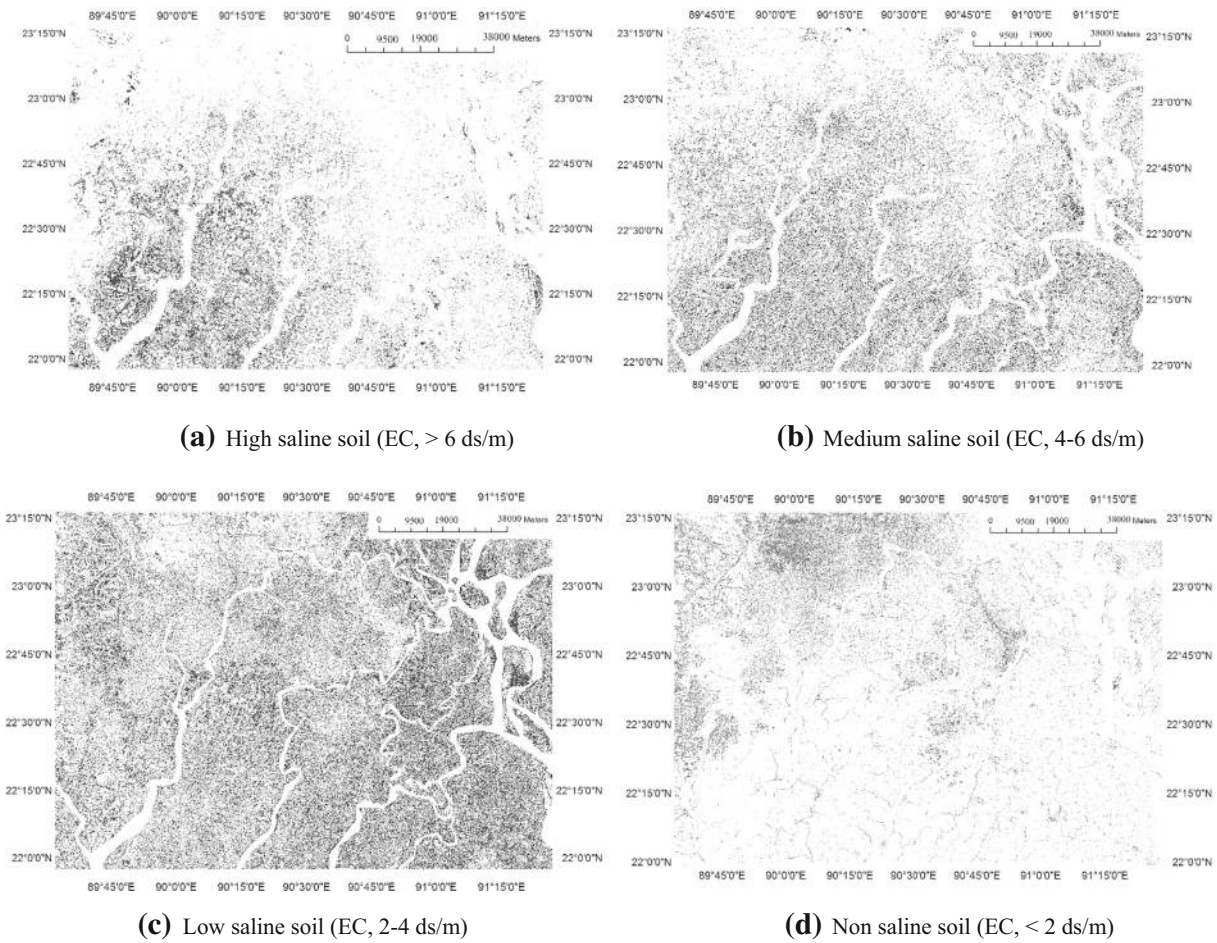

Fig. 8 Geographical location of different level of saline-affected soil. **a** High-saline soil (EC, >6 ds/m). **b** Medium-saline soil (EC, 4–6 ds/m). **c** Low-saline soil (EC, 2–4 ds/m). **d** Non-saline soil (EC, <2 ds/m)

sample size was too small. In addition, the temporal variation of the field data and satellite image influenced the accuracy of this salinity detection technique. The haze value correction could over-correct some pixel data. However, this integrated approach has the potential for detecting soil salinity over large area efficiently and economically.

Acknowledgments We would like to thank GB Wiersma, Editor-in-Chief, Environmental Monitoring and Assessment and anonymous reviewer's for their contribution in updating this paper.

Compliance with ethical standards

Ethical statement This is to confirm that the paper "Soil Salinity Detection Using Remote Sensing and GIS: An Integrated Approach of Salinity Indices and Field data" has been submitted to Environmental Monitoring and Assessment by the following ethical issues:

- The manuscript has submitted only in this journal and not published in any language before.
- All the data (primary and secondary) and results (image, graph, and table) used here was not manipulated.
- All the data, text, or theories by others used here have sufficiently are being acknowledged and referenced.
- All authors have consented to submission and publication in Environmental Monitoring and Assessment.
- All the authors contributed sufficiently to the work.
- The authors' affiliation institution is aware about this research and publication, and the research work was done under the direct supervision of the institution.
- This research does not deal with any human and animal species.
- The whole research was done on self-funding.
- This article does not contain any studies with human participants or animals performed by any of the authors.
- Informed consent was obtained from all individual participants included in the study.

Appendix

Table 5 Comparison of field EC and predicted EC in different geographical co-ordinate

Serial No.	Latitude	Longitude	Field EC	Predicted EC
1	22.70538	89.69170	1.11	1.52
2	22.70528	90.22582	6.49	8.42
3	22.70528	89.97511	5.34	7.42
4	22.70528	90.35960	1.72	2.02
5	22.96616	90.37238	5.77	4.86
6	22.34398	90.73842	8.86	7.04
7	23.19872	91.01022	2.27	1.62
8	23.38783	90.60608	1.17	1.37
9	23.08889	90.10493	1.01	1.08
10	23.33350	89.91290	1.62	1.54
11	22.83315	89.54620	1.69	0.61
12	22.83308	89.54623	2.01	2.62
13	22.83971	89.65009	1.59	1.50
14	22.88896	90.85750	7.58	5.08
15	22.93890	90.85323	0.80	1.52
16	22.69680	90.90979	6.05	3.55
17	23.11513	89.55514	1.18	1.225
18	22.82418	91.20047	0.77	1.13
19	22.46580	90.38599	1.17	2.60
20	22.47583	90.07568	4.44	3.53
21	23.11520	89.55492	1.40	2.30
22	23.11576	89.55485	1.18	1.62
23	23.11517	89.55520	1.03	1.22
24	23.11514	89.55519	2.18	1.22
25	23.11513	89.55514	0.70	1.225
26	23.33391	89.91295	1.68	1.67
27	23.08820	90.10508	0.90	1.43
28	23.38783	90.60611	1.02	0.96
29	23.38781	90.60612	1.44	0.96
30	23.19871	91.01031	1.55	1.62
31	23.34023	90.92264	1.03	1.49
32	23.34037	90.92214	1.31	1.21
33	22.70534	89.69180	1.59	1.52
34	22.93874	90.85358	0.50	1.38
35	22.93872	90.85318	0.60	1.21
36	22.93874	90.85358	0.70	1.388
37	22.83965	89.65006	2.27	1.308
38	22.70528	90.10717	10.47	9.58
39	23.08825	90.10497	0.90	1.65
40	22.83976	89.65017	4.10	3.42

References

Abdelfattah, M. A., Shahid, S. A., & Othman, Y. R. (2009). Soil salinity mapping model developed using RS and GIS—a case study from Abu Dhabi, United Arab Emirates. *European Journal of Scientific Research, 26*(3), 342–351.

Aldabaa, A. A. A., Weindorf, D.C., Chakraborty, S., Sharma, A., & Li, B. (2014). Combination of proximal and remote sensing methods for rapid soil salinity quantification. Geoderma, 239–240, 34–46. doi:10.1016/j.geoderma.2014.09.011.

Ben-Dor, E., Patkin, K., Banin, A., & Karnieli, A. (2002). Mapping of several soil properties using DAIS-7915 hyper spectral scanner data—a case study over clayey soils in Israel. *International Journal of Remote Sensing, 23*(6), 1043–1062.

Bishop, T. F. A., & McBratney, A. B. (2001). A comparison of prediction method for the creation of field-extent soil property maps. *Geoderma, 103*, 149–160.

Bouaziz, M., Matschullat, J., & Gloaguen, R. (2011). Improved remote sensing detection of soil salinity from a semi-arid climate in Northeast Brazil. *Comptes Rendus Geoscience, 343*, 795–803.

Carre, F., & Girard, M. C. (2002). Quantitative mapping of soil types based on regression-kriging of taxanomic distances with landform and land-cover attributes. *Geoderma, 110*, 241–263.

Chander, G., Markham, B.L., & Helder, D.L., (2009). Summary of current radiometric calibration coefficients for landsat MSS, TM, ETM+ and EO-1 ALI sensors. *Remote Sensing of Environment, 113*(5), 893–903.

Chavez, P. S., Jr. (1988). An improved dark-object subtraction technique for atmospheric scattering correction of multispectral data. *Remote Sensing of Environment, 24*, 459–479.

FAO. (2005). Management of irrigation-induced salt affected soils. Rome (Italy). CISEAU/FAO/IPTRID. ftp://ftp.fao.org/agl/agll/docs/salinity_brochure_eng.pdf.

Garcia, L., Eldeiry, A., & Elhaddad, A. (2005). Estimating soil salinity using remote sensing data. Proceedings of the 2005 Central Plains Irrigation Conference, 1–10.

Gupta, R. K., & Abrol, I. P. (1990). Salt-affected soils: their reclamation and management for crop production. *Advances in Soil Science, 11*, 223–288.

Hanson, R. B., Grattan, R. S., & Fulton, A. (2006). Agricultural salinity and drainage. Division of Agriculture and Natural Resources Publication. University of California, Davis. http://hos.ufl.edu/sites/default/files/faculty/gdliu/HansonGrattan2006_0.pdf.

Huang, C., Yang, L., Homer, C., Wylie, B., Vogelman, J., & DeFelice, T. (2002). At satellite reflectance: a first order normalization of LANDSAT 7 ETM+ images. http://landcover.usgs.gov/pdf/huang2.pdf.

Huete, A. R., Jackson, R. D., & Post, D. F. (1985). Spectral response of a plant canopy with different soil backgrounds. *Remote Sensing of Environment, 17*, 37–53.

Kassas, M. (1987). Seven paths to desertification. *Desertification Control Bulletin, 15*, 24–26.

Khaier, F.A. (2003). Soil salinity detection using satellite remote sensing. M.Sc. Thesis. International Institute for Geo-information Science and Earth Observation. www.itc.nl/library/papers_2003/msc/wrem/khaier.pdf.

Khan, T. M. A., Singh, O. P., & Rahman, M. S. (2000). Recent sea level rise and sea surface temperature trends along the Bangladesh coast in relation to the frequency of intense cyclones. *Marine Geodesy, 23*(2), 1–14.

Khan, N. M., Rastoskuev, V. V., Shalina, E., & Sato, Y. (2001). Mapping salt affected soil using remote sensing indicators. A simple approach with the use of GisIdrissi. 22nd Asian Conference on Remote Sensing, 5–9 November 2001, Singapore.

Li, D. J., Chun, W. M., & Tiyip, T. (2011). Study on soil salinization information in arid region using remote sensing technique. *Agricultural Science in China, 10*(3), 404–411.

Mashimbye, Z. E. (2013). Remote sensing of salt-affected soils. Ph.D. Thesis. Stellenbosch University. http://scholar.sun.ac.za/bitstream/handle/10019.1/79809/mashimbye_remote_2013.pdf.

Metternicht, G. I., & Zinck, J. A. (2003). Remote sensing of soil salinity: potentials and constraints. *Remote Sensing of Environment, 85*(1), 1–20.

Nwer, B., Zurqani, H., & Rhoma, E. (2013). The use of remote sensing and geographic information system for soil salinity monitoring in Libya. *GSTF International Journal of Geological Sciences, 1*(1), 1–5.

Ortiz, C. A. C. (1994). Sea level rise and its impact on Bangladesh. *Ocean Coast Management, 23*, 249–270.

Schofield, R., Thomas, D. S. G., & Kirby, M. J. (2001). Casual processes of soil salinization in Tunisia, Spain and Hungary. *Land Degradation & Development, 12*(2), 163–181.

Singh, O. P., Khan, A. T. M., Murty, T. S., & Rahaman, M. S. (2001). Sea level changes along Bangladesh coast in relation to southern oscillation phenomenon. *Marine Geodesy, 24*(1), 65–72.

Soil Resource Development Institute (SRDI). (2010). Saline soils of Bangladesh. Dhaka, Bangladesh. Ministry of Agriculture, Government of Bangladesh.

Vermote, E. F., Nazmi, Z., Saleous, E., & Christopher, O. (2002). Atmospheric correction of MODIS data in the visible to middle infrared: first results. *Remote Sensing of Environment, 83*, 97–111.

World Bank. (2000). Bangladesh—Climate change and sustainable development. Washington, DC. World Bank. http://documents.worldbank.org/curated/en/2000/12/1047483/bangladesh-climate-change-sustainable-development.

Wu, J., Vincent, B., Yang, J., Bouarfa, S., & Vidal, A. (2008). Remote sensing monitoring of changes in soil salinity: a case study in Inner Mongolia, China. *Sensors, 8*(11), 7035–7049.